Published OnlineFirst February 18, 2019; DOI: 10.1158/0008-5472.CAN-18-1544

Tumor Biology and Immunology

Cancer Research

Nicotinamide Phosphoribosyltransferase Acts as a Metabolic Gate for Mobilization of Myeloid-Derived Suppressor Cells

Cristina Travelli[1,2], Francesca Maria Consonni[3], Sabina Sangaletti[4], Mariangela Storto[3], Sara Morlacchi[3], Ambra A. Grolla[1], Ubaldina Galli[1], Gian Cesare Tron[1], Paola Portararo[4], Lorenza Rimassa[5], Tiziana Pressiani[5], Massimiliano Mazzone[6], Rosalinda Trovato[7], Stefano Ugel[7], Vincenzo Bronte[7], Claudio Tripodo[8,9], Mario P. Colombo[4], Armando A. Genazzani[1], and Antonio Sica[1,3]

Abstract

Cancer induces alteration of hematopoiesis to fuel disease progression. We report that in tumor-bearing mice the macrophage colony-stimulating factor elevates the myeloid cell levels of nicotinamide phosphoribosyltransferase (NAMPT), the rate-limiting enzyme in the NAD salvage pathway, which acts as negative regulator of the CXCR4 retention axis of hematopoietic cells in the bone marrow. NAMPT inhibits CXCR4 through a NAD/Sirtuin 1–mediated inactivation of HIF1α-driven *CXCR4* gene transcription, leading to mobilization of immature myeloid-derived suppressor cells (MDSC) and enhancing their production of suppressive nitric oxide. Pharmacologic inhibition or myeloid-specific ablation of NAMPT prevented MDSC mobilization, reactivated specific antitumor immunity, and enhanced the antitumor activity of immune checkpoint inhibitors. Our findings identify NAMPT as a metabolic gate of MDSC precursor function, providing new opportunities to reverse tumor immunosuppression and to restore clinical efficacy of immunotherapy in patients with cancer.

Significance: These findings identify NAMPT as a metabolic gate of MDSC precursor function, providing new opportunities to reverse tumor immunosuppression and to restore clinical efficacy of immunotherapy in cancer patients.

Introduction

Perturbation of myelopoiesis in cancer (1, 2) leads to the expansion of a heterogeneous population of immunosuppressive immature myeloid cells, called myeloid-derived suppressor cells (MDSC), comprising the monocytic (M-MDSC) and granulocytic (PMN-MDSC) subsets (3, 4). Along with tumor-associated macrophages (5), these cells are negative regulators of anticancer immune responses and are considered major promoters of tumor immune evasion, metastasis formation, and cancer cell "stemness" (6–8). In addition, MDSCs produce endothelial growth factors (e.g., VEGF, bFGF) and proinflammatory cytokines involved in neoangiogenesis and tumor promotion. MDSCs originate from a common myeloid precursor (CMP) in pathologic conditions such as cancer (6) and their accumulation in the periphery (e.g., blood, lymph nodes, spleens, tumors) correlates with tumor stage and clinical outcome (9). Mobilization of MDSC precursors from the bone marrow hematopoietic environment to the periphery is tightly controlled by the retention axis CXCR4/CXCL12 (10) and pharmacologic inhibitors of CXCR4 are now under clinical investigation for the mobilization of immune and hematopoietic stem cells (11). Noteworthy, depletion of MDSCs by chemotherapeutic agents (e.g., gemcitabine, cyclophosphamide) can efficiently contribute to their anticancer action (6, 12–14). Although little is known regarding the connection between MDSC metabolism and cancer-related immunosuppression, metabolic fluxes have been recently indicated as novel therapeutic targets for the restoration of anticancer immunosurveillance (15). Nicotinamide phosphoribosyltransferase (NAMPT) is the rate-limiting enzyme in the nicotinamide adenine dinucleotide (NAD) salvage pathway, converting nicotinamide into nicotinamide mononucleotide (NMN), precursor of NAD (16). NAD plays a crucial role in maintaining cellular energy by redox reactions and is actively consumed by NAD-dependent enzymes [e.g., sirtuins, mono and poly (ADP-ribose) polymerase/ARTs and CD38/CD157; ref. 17]. In particular, NAD promotes the expression of the deacetylase Sirtuin 1 (SIRT1), which in turn represses

[1]Department of Pharmaceutical Sciences, University of Eastern Piedmont, Novara, Italy. [2]Department of Pharmaceutical Sciences, University of Pavia, Pavia, Italy. [3]Department of Inflammation and Immunology, Humanitas Clinical and Research Center, Rozzano, Milan, Italy. [4]Department of Research, Fondazione IRCCS Istituto Nazionale dei Tumori, Milano, Italy. [5]Medical Oncology and Hematology Unit, Humanitas Cancer Center, Humanitas Clinical and Research Center, Rozzano, Milan, Italy. [6]Laboratory of Tumor Inflammation and Angiogenesis, Department of Oncology, Vesalius Research Center, VIB, Leuven, Belgium. [7]Department of Medicine, Section of Immunology, University of Verona, Verona, Italy. [8]Human Pathology Section, Department of Health Sciences, University of Palermo, Palermo, Italy. [9]Tumor and Microenvironment Histopathology Unit, the FIRC Institute of Molecular Medicine (IFOM), Milan, Italy.

Note: Supplementary data for this article are available at Cancer Research Online (http://cancerres.aacrjournals.org/).

Corresponding Authors: Antonio Sica, University of Eastern Piedmont Amadeo Avogadro, Largo Donegani 2, Novara 28100, Italy. Phone: 3903-2137-5881; Fax: 3903-2137-5621; E-mail: antonio.sica@uniupo.it; and Armando A. Genazzani, armando.genazzani@uniupo.it

doi: 10.1158/0008-5472.CAN-18-1544

©2019 American Association for Cancer Research.

Downloaded from cancerres.aacrjournals.org on February 4, 2020. © 2019 American Association for Cancer Research.

Published OnlineFirst February 18, 2019; DOI: 10.1158/0008-5472.CAN-18-1544

HIF1α transcriptional activity (18). Of relevance, SIRT1 was shown to promote M2 polarization and suppressive activity of MDSCs (19). Therefore, as a biosynthetic enzyme of NAD, NAMPT affects a variety of metabolic and stress responses, through modulation of distinct transcriptional activities. NAMPT expression increases in various diseases, including chronic inflammatory conditions (e.g., rheumatoid arthritis), metabolic alterations (e.g., diabetes), and cancer (20). NAMPT inhibitors have entered clinical trials for solid and nonsolid tumors, due to their ability in lowering NAD and ATP levels and, in turn, interfering with malignant cell growth (20). Despite this evidence (5, 21), the contribution of NAMPT in cancer-related inflammation remains elusive (22). Given that reprogramming of energy and amino acid metabolism (e.g., tryptophan/arginine) is an essential event in tumor-related immunosuppression (5), this study was designed to elucidate the role of NAMPT in the function and fate of MDSCs.

Materials and Methods

Patients

Peripheral blood (20 mL) were collected from healthy donors and patients with T2/T3 colorectal cancer, stratified on Ficoll gradient, and 1×10^6 cells were stained at 4°C for 30 minutes with a cocktail of mAbs (See Supplementary Material). An anti-Nampt was used followed by incubation with goat anti-mouse Alexa Fluor 647 antibody. For intracellular staining, Foxp3/Transcription Factor Staining Buffer Set was used according to the manufacturer's instruction. Cells were detected using the BD FACSCanto II cytofluorimeter and analyzed with FlowJo Software. M-MDSCs were identified within the gate of HLA-DR$^{low/neg}$ cells as CD33^{high}CD14$^+$ cells, whereas monocytes were HLA-DR$^+$CD14$^+$CD33^{high}. We have obtained written informed consent from the patients and the study was approved by the institutional review board and conducted in accordance with recognized ethical guidelines (e.g., Declaration of Helsinki).

Drugs

FK866 and MV87 have been synthetized as described previously (patent WO/2014/178001; ref. 23), dissolved in DMSO at 10 mmol/L, and kept at −20°C. ADM3100 was purchased from Sigma-Aldrich.

Animals

The study was approved by the scientific board and ethics committee of the University of Eastern Piedmont (Novara, Italy). Mice have been monitored daily and euthanized when displaying excessive discomfort or any signs of pain. All experiments involving animals described in this study were approved by the Ministry of Health (authorization number 245/2018-R). The protocols describing the generation of NAMPT, HIF1α, and SIRT1 conditional KO mice, as well as thymectomy, are described in the Supplementary Data.

Syngeneic orthotopic fibrosarcoma and mammary carcinoma mouse models

The MN/MCA1 cells (WT, WT-NAMPT or G217R-NAMPT) were isolated from spontaneous fibrosarcoma by methylcholanthrene-treated mice and propagated in RPMI with 10% FBS, 2 mmol/L L-glutamine and 10 μg/mL penicillin–streptomycin (2). The 4T1 cells (ATCC, CRL-2539; ref. 24) were maintained in DMEM with 10% FBS, 2 mmol/L L-glutamine, and 10 μg/mL penicillin–streptomycin. MN/MCA1 cells (10^4/10^5) were inoculated intramuscularly in 8 weeks old male C57BL/6 mice (Charles River) or in NAMPT$^{f/f}$LysMCre$^{-/-}$ or in NAMPT$^{f/f}$LysMCre$^{+/-}$. A total of 7×10^3 4T1 cells were injected in the fat pad of 8 weeks old female BALB/c mice using a 26-gauge needle. From day 1, mice were treated intraperitoneally with either vehicle (PBS + 10% DMSO, twice daily), FK866 or MV87 (10 mg/kg in PBS + 10% DMSO, twice daily), or ADM3100 (3 mg/kg, i.p, every 3 days). Starting from day 15, tumor growth was monitored using a caliper. At the sacrifice, blood was collected, mice were sacrificed and spleen, bone marrow, primary tumors, and lungs collected. Tumors weights were monitored, lungs were washed in PBS, and lung metastasis counted. Authentication of cell lines was not performed; all cell lines were tested for *Mycoplasma* infection using PCR system and only cells at 1–4 passages were used.

Proliferation assay

M-MDSCs (Ly6C^{hi}Ly6G$^-$ cells) isolated from the spleen of tumor-bearing mice were plated in 96 wells at 24% of total cells, in presence of splenocytes from OT-I transgenic mice, labeled with 1 μmol/L CellTrace (Thermo Fisher Scientific) and diluted 1:10 with CD45.1$^+$ splenocytes, in the presence of SIINFEKL peptide (1 μg/mL). After 3 days, cells were stained with APC-Cy7–conjugated anti-CD45.2 and PerCP-Cy5.5–conjugated anti-CD8. CellTrace signal of gated lymphocytes was used to analyze cell proliferation using the following formula 1 − (% proliferation with MDSCs/% proliferation without MDSCs) × 100. Samples were acquired with FACSCanto II (BD Biosciences). Cell proliferation was also estimated by 3[H]-thymidine incorporation, as described in the Supplementary Section.

Antibody treatments *in vivo*

The anti-PD-1 antibody was given at 200 μg twice a week, starting 9 days after tumor cells' injection. CSF1R antagonist (or isotype control) was administered as an initial dose of 60 mg/kg followed by two doses of 30 mg/kg two times a week for a total of 2 weeks.

Histology and IHC

Mouse tissues were collected for fixation in 10% neutral buffered formalin and included in paraffin. Bone marrow samples were decalcified for 8 hours using an EDTA-based decalcifying solution, washed in flowing water (1 hour), and subsequently processed and embedded in paraffin. Four-micron–thick sections were deparaffinized, rehydrated, and stained with hematoxylin and eosin for histopathologic analyses or with IHC. The antigen unmasking was performed using Novocastra Epitope Retrieval Solutions pH6 and pH9 in a PT Link Dako pretreatment module (Dako) at 98°C for 30 minutes. After neutralization of the endogenous peroxidases with 3% H_2O_2 and Fc blocking by a specific protein block (Novocastra), samples were incubated with: CD8a or CXCR4 or IL4R or CD3 and the staining was revealed using goat anti-rat IgG or donkey anti-rabbit and AEC (3-Amino-9-ethylcarbazole) substrate-chromogen (Dako). Slides were analyzed under a Zeiss Axioscope A1 and microphotographs collected using a Zeiss Axiocam 503 Color with the Zen 2.0 Software (Zeiss). Quantitative IHC data were obtained by counting the number of immunoreactive cells out of four microscopic (×400 magnification).

Downloaded from cancerres.aacrjournals.org on February 4, 2020. © 2019 American Association for Cancer Research.

Published OnlineFirst February 18, 2019; DOI: 10.1158/0008-5472.CAN-18-1544

Cell culture

Bone marrow–derived MDSCs. Bone marrow cells were obtained from the femurs and tibias, 2×10^6cells were cultured for 4 days in RPMI1640 containing 10% FBS, 2 mmol/L glutamine, 100 U/mL penicillin–streptomycin, 10 mmol/L HEPES, 20 μmol/L β-mercaptoethanol, 40 ng/mL of rmIL6, rmG-CSF, and rmGM-CSF. When needed, bone marrow–derived M- and PMN-MDSCs were sorted using a BD FACSAria III Cell sorter with the following antibodies: CD11b-PerCp-Cy5.5, Ly6C-APC, Ly6G-PE (post-sort cells were 98.9% ± 0.5% pure).

Spleen-derived M- and PMN-MDSCs. Cells were isolated by MACS cell separation according to the manufacturer's instructions. MDSCs were first enriched by serial negative selections with $CD19^+$ and $CD11c^+$ microbeads and then $Ly6G^+$ cells were positively selected with Ly6G microbeads kit. Remaining cells were positively selected with $CD11b^+$ microbeads, which all stained positive for Ly6C marker. The purity of populations was >90% (by flow cytometry). The concentration for the different treatments were as follows: murine IFNγ 200 U/mL, murine IL4 20 ng/mL, LPS from Salmonella Abortus Equi S-form 100 ng/mL, MV87 10 nmol/L, and FK866 10 nmol/L. Nitric oxide (NO) and reactive oxygen species (ROS) production were determined as described in Supplementary Section.

Bone marrow–derived macrophages. $Csf3r^{-/-}$ bone marrow–derived macrophages were obtained by culturing for 6 days bone marrow–derived cells (3.5×10^6/mL) in RPMI1640 medium with 10% FBS, 2 mmol/L glutamine, 100 U/mL penicillin–streptomycin, and macrophage colony-stimulating factor (M-CSF; 20 ng/mL).

Bone marrow $CD11b^+$ cells. $CD11b^+$ cells (purity ≥98%) were positively selected from total bone marrow cells of naïve WT mice and tumor-bearing mice treated or not with anti-CSF1R with $CD11b^+$ microbeads.

Flow cytometry

Blood cells were collected from the eye vein of anesthetized mice and splenocytes from spleen after filtration through cell strainers (70 μm). Bone marrow cells were obtained from femurs and tibias. Primary tumors were cut and disaggregated with collagenase (0.5 mg/mL) and with MACS dissociator. Cells (10^6) were resuspended in Hank's Balanced Salt Solution with 0.5% BSA and the staining was performed at 4°C for 20 minutes with specific antibodies (see Supplementary Section). When required, Annexin-V/PI staining was performed. Cell viability was determined by LIVE/DEAD Fixable Violet Dead Cell Stain Kit. For intracellular staining, Foxp3/Transcription Factor Staining Buffer Set was used according to the manufacturer's instructions. Cells were detected using the BD FACSCanto II, BD LSRFortessa or BD Accuri C6 and analyzed with BD FACSDiva and FlowJo (9.3.2) software.

Viability assay

Viability of cells was measured using the 3-(4,5-dimethylthiazol-2-yl)-2,5-diphenyltetrazolium assay after the treatments with FK866 or MV87 (1–1,000 nmol/L) for 48 hours. In parallel, the Annexin-V/PI staining was performed according to the manufacturer's instructions.

Gene expression

The levels of gene expression were determined by RT-PCR as described in the Supplementary Section.

Statistical analysis

For animal studies, the size of each experimental group was defined to detect differences of 20% or greater between groups. Statistics were calculated with GraphPad Prism version 6 software. The two-sided unpaired Student t test was used to compare unmatched groups and expressed as *, $P < 0.05$; **, $P < 0.01$; ***, $P < 0.001$.

Results

NAMPT promotes tumor growth and expansion of MDSCs

To investigate the mechanisms underlying the tumor-promoting activity of NAMPT (20), we used the transplantable MN/MCA1 fibrosarcoma mouse model (2) and tested the antitumor efficacy of two distinct NAMPT inhibitors, FK866 (20) and MV87 (23). Treatment of MN/MCA1 cells *in vitro* (48 hours) with either FK866 or MV87 resulted in pronounced cell death, assessed either by the colorimetric MTT assay (Supplementary Fig. S1A) or Annexin-V/PI staining (Supplementary Fig. S1B). Subsequently, C57BL/6 mice were injected intramuscularly in the hind limb with 10^4 MN/MCA1 cells and treated with FK866 or MV87 (10 mg/kg, twice daily). Both NAMPT inhibitors delayed fibrosarcoma tumor growth *in vivo*, in terms of tumor volume (Supplementary Fig. S1C), weight (Supplementary Fig. S1D), and inhibition of spontaneous lung metastasis formation, assessed when the tumor volume was 2.5 cm^3 (Supplementary Fig. S1E). As myeloid cells are master orchestrators of tumor-promoting inflammation, we analyzed the prevalence of different myeloid populations in tumor-bearing mice. MV87 significantly reduced the number of M-MDSCs ($CD45^+CD11b^+Ly6C^{high}Ly6G^{low}$) and PMN-MDSCs ($CD45^+CD11b^+Ly6C^{low}Ly6G^{high}$) in the peripheral blood, spleen, and primary tumor (Supplementary Fig. S1F). In contrast, $CD45^+CD11b^+MHCII^+CD11c^+Ly6C^-$ dendritic cells and $CD45^+F4/80^+$ monocytes/macrophages remained unaffected in the tumor (Supplementary Fig. S1F). Moreover, MV87 treatment significantly increased the number of $CD45^+CD3^+$ T and $CD45^+CD8^+$ T cells within the primary tumor, spleen, and peripheral blood, whereas the levels of $CD45^+CD4^+$ T cells increased in both the blood and the primary tumor (Supplementary Fig. S1G). A 2-fold increase in the number of $IFN\gamma^+CD8^+$ T cells was found in tumors of MV87-treated mice, whereas the levels of both $IFN\gamma^+CD4^+$ and Treg ($Foxp3^+/CD4^+$) cells were unaffected (Supplementary Fig. S1H). The *in vivo* effects of MV87 were confirmed in the mammary adenocarcinoma 4T1 model, in which NAMPT inhibition impaired both tumor growth and lung metastases (Supplementary Fig. S1I). These effects were coupled with a reduced expansion of both M-MDSCs and PMN-MDSCs in the spleen and in primary tumor, but not in the peripheral blood, and were paralleled by the increased tumor infiltration of $CD3^+$ T cells (Supplementary Fig. S1J).

NAMPT inhibition releases MDSC restraints over antitumor immunity and synergizes with immune checkpoint inhibition

To dissect the antitumor activity of NAMPT inhibitors through either direct tumor cell cytotoxicity or reactivation of antitumor immunity, we generated inhibitor-resistant MN/MCA1 cells overexpressing the G217R-point–mutated *Nampt* gene (25), which

Downloaded from cancerres.aacrjournals.org on February 4, 2020. © 2019 American Association for Cancer Research.

Published OnlineFirst February 18, 2019; DOI: 10.1158/0008-5472.CAN-18-1544

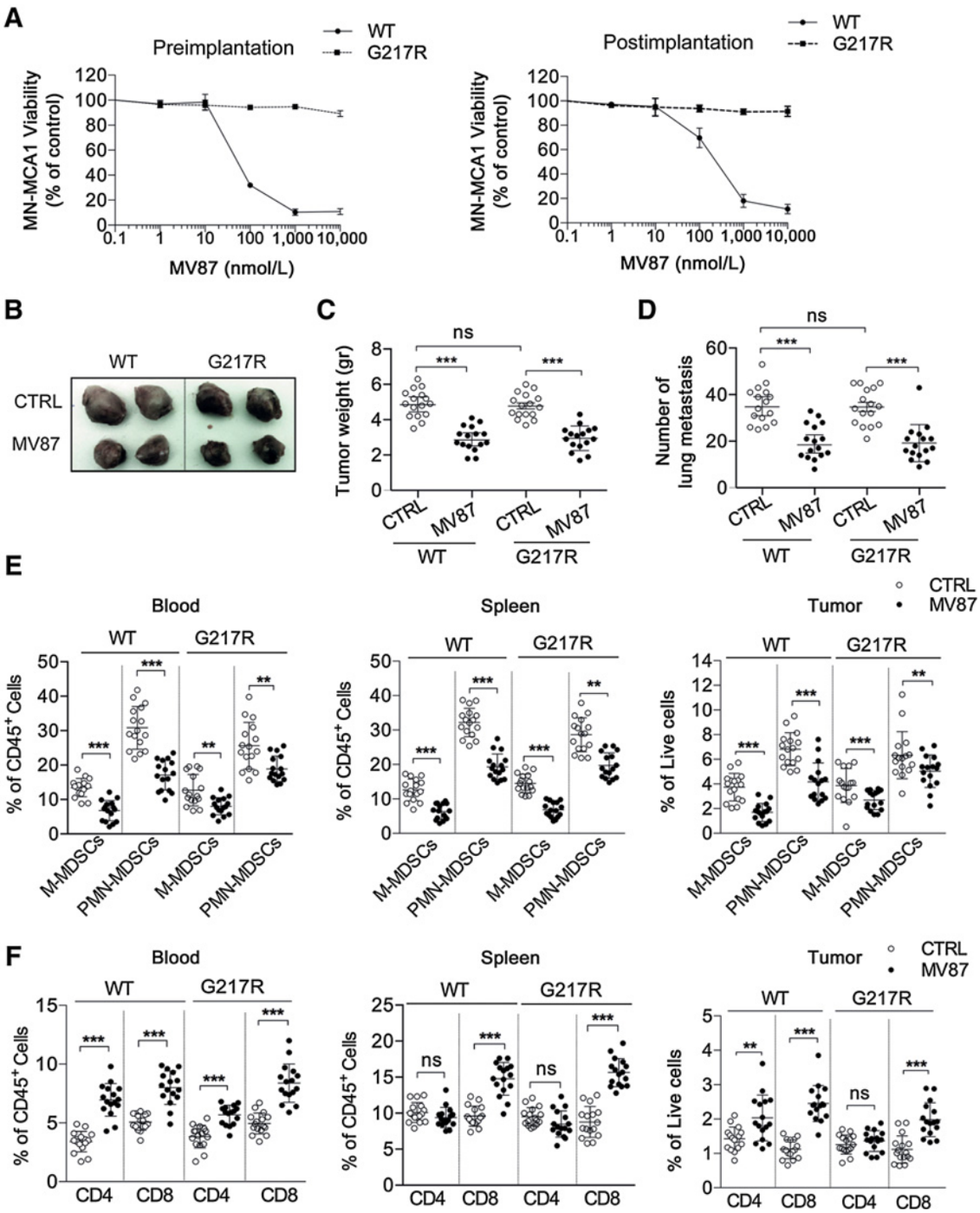

Figure 1.

Effects of NAMPT inhibitors on leukocyte populations of tumor-bearing mice. **A,** Tumor cell viability (MTT assay) of WT MN/MCA1 and G217R-MN/MCA1 cells in the presence or absence of MV87 for 48 hours. Left, preimplantation; right, postimplantation. Mean percentages ± SD of three ($n = 12$) and two ($n = 8$) independent experiments, respectively. **B,** WT MN/MCA1 and G217R-MN/MCA1 growth in mice treated with vehicle or MV87 (10 mg/kg). Representative image of untreated and MV87-treated WT-MN/MCA1 and G217R-MN-MCA1 tumors. **C,** Weight of tumors (gr) in mice treated as indicated. Mean percentages ± SD of two independent experiments (8 mice/group). **D,** Lung metastasis number in WT MN/MCA1 and G217R-MN/MCA1 tumor-bearing mice. Mean percentages ± SD of two independent experiments (8 mice/group). **E,** Mean percentage ± SD of M-MDSCs ($CD45^+CD11b^+Ly6G^{low}Ly6C^{high}$) and PMN-MDSCs ($CD45^+CD11b^+Ly6G^{high}Ly6C^{low}$) in blood, spleen, and tumors from vehicle (CTRL) or MV87-treated WT MN/MCA1 and G217RMN/MCA1 tumor-bearing mice. Mean percentages ± SD of two independent experiments (8 mice/group). **F,** Mean percentage ± SD of $CD4^+$ T cells ($CD45^+CD4^+$) and $CD8^+$ T cells ($CD45^+CD8^+$) in blood, spleen, and tumors from vehicle or MV87-treated WT MN/MCA1 or G217RMN/MCA1 tumor-bearing mice. Mean percentages ± SD of two independent experiments (8 mice/group; *t* test; **, $P < 0.01$; ***, $P < 0.001$). ns, nonsignificant.

Downloaded from cancerres.aacrjournals.org on February 4, 2020. © 2019 American Association for Cancer Research.

Published OnlineFirst February 18, 2019; DOI: 10.1158/0008-5472.CAN-18-1544

prevents the binding of NAMPT inhibitors to the enzyme while preserving its enzymatic activity. A WT-*Nampt*-MN/MCA1 cell line overexpressing the WT-*Nampt* gene was used as a control. As expected, *Nampt*^{G217R}, but not *Nampt*^{WT}, MN/MCA1 cells, were refractory to the *in vitro* treatment with MV87 (Fig. 1A, left). Strikingly, despite the sole *Nampt*^{G217R}-MN/MCA1 cells' resistance to NAMPT inhibitors, treatment with MV87 effectively reduced tumor growth and metastasis formation *in vivo*, of both *Nampt*^{WT}- and *Nampt*^{G217R}-MN/MCA1 cell implants (Fig. 1B–D). Considering that *Nampt*^{G217R}-MN/MCA1 cells isolated *ex vivo* (postimplantation) from established tumors maintained their refractoriness to MV87 treatment (Fig. 1A, right), the data demonstrated a tumor cell–extrinsic effect of MV87. Accordingly, we observed that the treatment with MV87 reduced M-MDSC and PMN-MDSC cell number, in peripheral blood, spleen, and primary tumors (Fig. 1E), which was associated with an increase in the number of $CD4^+$ and $CD8^+$ T cells in both *Nampt*^{WT}- and *Nampt*^{G217R}-MN/MCA1–bearing mice (Fig. 1F).

To further confirm that NAMPT inhibition mediates antitumor activity by limiting MDSCs hijacking adaptive immunity, 6-week-old mice were subjected to thymectomy and treated with anti-CD4 and anti-CD8 antibodies, to deplete T lymphocyte populations (2). In athymic mice, the antitumor efficacy of MV87 was blunted (Fig. 2A–C), indicating that reactivation of antitumor-specific immunity was the major effector of the anticancer activity of MV87. In agreement, MV87 reduced the levels of MDSCs in the peripheral blood, spleen, and primary tumors (Fig. 2D). As a large number of patients present or develop with resistance to anticancer immunotherapies, including immune checkpoint inhibitors, we next addressed whether NAMPT inhibition could enhance the efficacy of anti-PD-1 immunotherapy (26). As result, treatment of fibrosarcoma with the combination of an anti-PD-1 antibody and MV87 displayed a significantly higher antitumor activity as compared with the single treatments (Fig. 2E). Next, to investigate the myeloid-specific activity of NAMPT, we developed a mouse model carrying a specific deletion of the *Nampt* gene in the myeloid compartment (NAMPT$^{f/f}$LysMCre$^{+/-}$). As compared with the NAMPT$^{f/f}$ control mice, analysis of NAMPT protein levels in different tissues from tumor-free NAMPT$^{f/f}$LysMCre$^{\pm}$ mice showed a 40% reduction in total bone marrow (Supplementary Fig. S2A and S2B), along with a 70% and 45% decrease in bone marrow–derived M-MDSCs and PMN-MDSCs, respectively (Supplementary Fig. S2C). A similar decrease was observed in the *Nampt* mRNA levels of BM-M-MDSCs ($CD45^+CD11b^+Ly6G^{low}Ly6C^{high}$) and BM-PMN-MDSCs ($CD45^+CD11b^+Ly6G^{high}Ly6C^{low}$) derived from NAMPT$^{f/f}$-CreLysM$^{+/-}$ mice (Supplementary Fig. S2D).

Confirming the protumoral activity of myeloid-specific NAMPT, MN/MCA1 tumor volume (Fig. 3A), weight (Fig. 3B), and metastasis formation (Fig. 3C) were significantly reduced in NAMPT$^{f/f}$LysMCre$^{\pm}$ mice, as compared with NAMPT$^{f/f}$ controls. The prevalence of myeloid subsets recruited into tumors of NAMPT$^{f/f}$LysMCre$^{\pm}$ mice was concordant with that found following treatment with NAMPT inhibitors (Supplementary Fig. S1). Indeed, myeloid-specific deletion of NAMPT did not alter the percentage of both $CD45^+F4/80^+$ macrophages and $CD45^+CD11b^+MHCII^+CD11c^+Ly6C^-$ dendritic cells in the tumor (Fig. 3D), which, however, was defective in the M-MDSCs in the peripheral blood, spleen, and primary tumors and reduced in circulating PMN-MDSCs. Notably, the number of $CD3^+$ and $CD8^+$ T lymphocytes in blood and primary tumors (Fig. 3E), as well as the number of tumor-infiltrating $IFN\gamma^+CD8^+$ T cells (Fig. 3F), was increased in NAMPT$^{f/f}$LysMCre$^{\pm}$ mice, leaving the number of $CD4^+$ T cells (Fig. 3E), IFN-γ^+CD4^+, and Tregs ($Foxp3^+CD4^+$; Fig. 3F) unaltered, while the $CD44^+CD62L^-$ effector/memory $CD8^+$ T-cell populations were increased in both spleen and tumor from NAMPT$^{f/f}$LysMCre$^{\pm}$ mice (Fig. 3G). These results suggest that NAMPT inhibition reduces tumor outgrowth by limiting the expansion of tumor-promoting MDSCs and promoting T-cell infiltration. To further support NAMPT as a myeloid-specific target to improve cancer immunotherapy, NAMPT$^{f/f}$ and NAMPT$^{f/f}$LysMCre$^{\pm}$ fibrosarcoma-bearing mice were treated with the anti-PD-1 mAb. Moreover, myeloid-specific ablation of NAMPT reinforced the antitumor activity of anti-PD-1 treatment, on both primary and secondary lung metastasis (Fig. 3H–J).

NAMPT contributes to MDSC immunosuppressive competence

In light of the renewed anticancer immunity subsequent to the inhibition of myeloid NAMPT, we investigated its influence on the energy metabolism of MDSCs. Evidences indicate that M1-polarizing signals promote expression of the immunosuppressive enzyme inducible nitric oxide synthase (iNOS; ref. 6) and guide the metabolic reprogramming of myeloid cells with increased NADH:NAD^+ redox potential and reduced oxygen consumption (27). On these bases, we investigated both NAMPT expression and NAD levels in resting and IFNγ-stimulated splenic MDSCs, isolated from tumor-bearing WT animals. As compared with PMN-MDSCs, M-MDSCs expressed higher levels of *Nampt* mRNA (Supplementary Fig. S3A), which, however, was strongly induced in both cell types by IFNγ and/or LPS (Supplementary Fig. S3B). In agreement, NAMPT protein level was increased by IFNγ in bone marrow–derived M- and PMN-MDSCs, whereas neither the NAMPT inhibitor FK866 nor the M2-polarizing signals IL10 and IL4 were able to affect NAMPT expression (Supplementary Fig. S3C and S3D). Analysis of additional key immunosuppressive genes in *Nampt*-deficient MDSCs showed that, as compared with their parental counterparts, M-MDSCs from NAMPT$^{f/f}$LysMCre$^{\pm}$ mice were less efficient in inducing iNOS and NADPH oxidase (NOX2) expression in response to IFNγ (Supplementary Fig. S3E), while no differences were observed in the expression of NOX2, Arginase I, and Indoleamine 2,3-dioxygenase (IDO) by PMN-MDSCs (Supplementary Fig. S3F). The intracellular role of NAMPT is to catalyze the formation of NMN, the precursor of NAD, representing the bottleneck enzyme of NAD biosynthesis (16). Treatment with FK866 or MV87 induced a significant drop in NAD and ATP levels in untreated and IFNγ-activated BM-MDSCs, whereas compared with NAMPT$^{f/f}$ BM-MDSCs, a similar reduction was observed in NAMPT$^{f/f}$LysMCre$^{\pm}$ BM-MDSCs (Supplementary Fig. S3G and S3H). The observed IFNγ-induced increase of NAD (60%) and ATP levels (40%) suggested a link between the metabolic reprogramming of MDSCs and their suppressive activity.

To test the role of NAMPT in the suppressive functions of MDSCs, BM-MDSCs were treated *in vitro* with NAMPT inhibitors (10 nmol/L) and tested for the production of the suppressive molecules NO and ROS, by M-MDSCs and PMN-MDSCs, respectively (6). Neither FK866 nor MV87 inhibited the production of ROS by PMA/ionomycin–activated BM-PMN-MDSCs (Supplementary Fig. S4A). On the contrary, MV87 markedly inhibited NO production by IFNγ-treated splenic-M-MDSCs (Supplementary Fig. S4B). Subsequently, splenic M-MDSCs from vehicle or MV87-treated tumor-bearing mice were activated with IFNγ,

Downloaded from cancerres.aacrjournals.org on February 4, 2020. © 2019 American Association for Cancer Research.

Published OnlineFirst February 18, 2019; DOI: 10.1158/0008-5472.CAN-18-1544

loaded with ovalbumin and then cocultured for three days with total splenocytes purified from OT-1 transgenic mice, expressing the T-cell receptor–specific for the ovalbumin antigen. As a result, M-MDSCs from MV87-treated mice displayed reduced suppressive activity, estimated as proliferation of cocultured OT1 splenocytes (Supplementary Fig. S4C). In agreement, myeloid-specific ablation of NAMPT (NAMPT$^{f/f}$LysMCre$^{+/-}$) did not affect the ROS production by BM-PMN-MDSCs (Supplementary Fig. S4D), whereas splenic M-MDSCs from NAMPT$^{f/f}$LysMCre$^{\pm}$ displayed reduced NO production (Supplementary Fig. S4E) and suppressive activity (Supplementary Fig. S4F) in response to IFNγ treatment, as compared with splenic M-MDSCs from NAMPT$^{f/f}$ tumor-bearing mice. Consistently, the suppressive activity of splenic M-MDSCs isolated from tumor-bearing mice treated with the NAMPT inhibitor MV87 was abolished also in the absence of exogenous IFNγ (Fig. 4SG).

To demonstrate the *in vivo* role of NO production in tumor development, tumor-bearing mice (MN/MCA1) were treated with

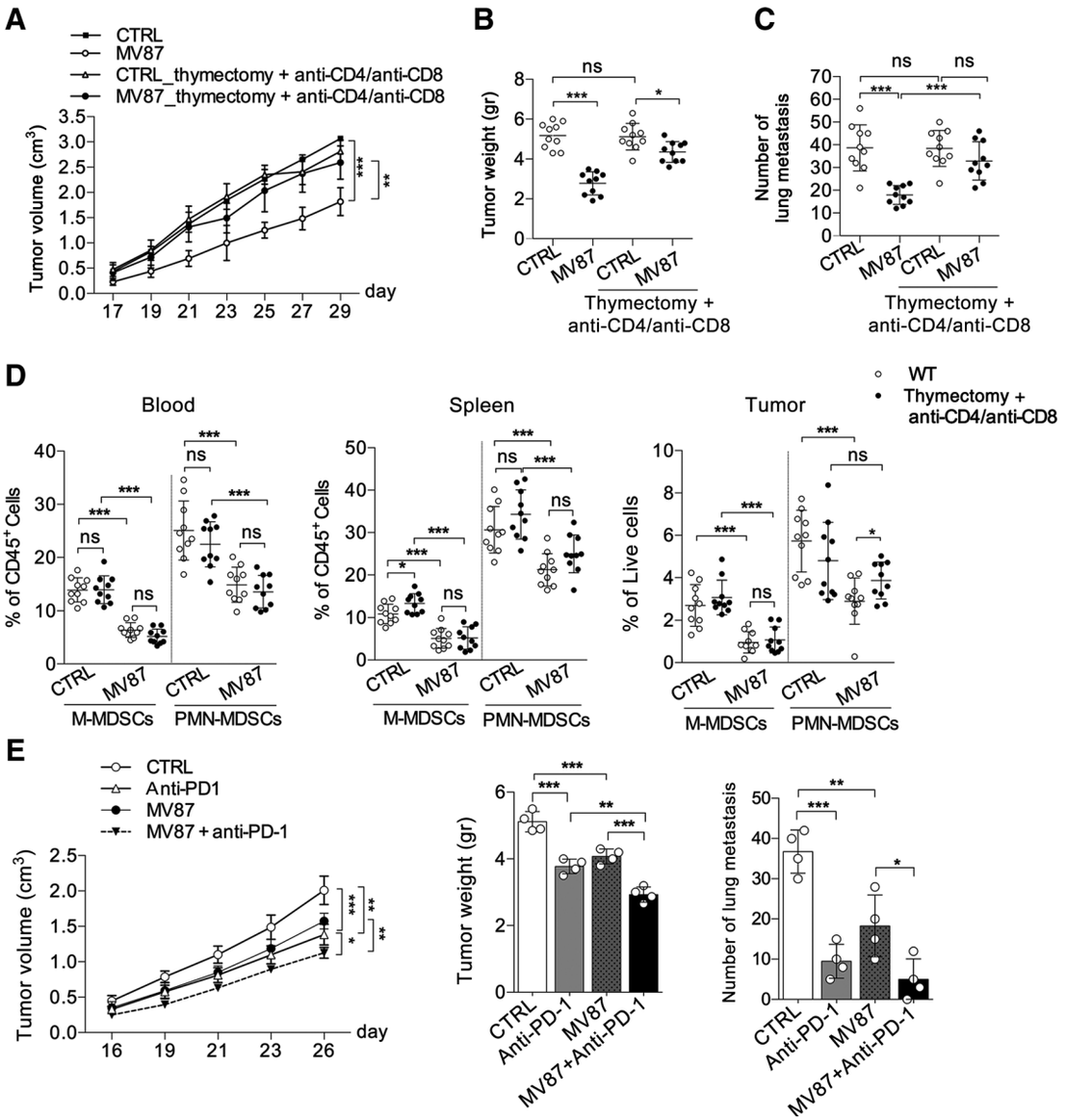

Figure 2.

NAMPT inhibition restores specific antitumor immunity. **A,** MN/MCA1 growth in WT naïve or athymic mice, depleted of T lymphocyte populations (anti-CD4/anti-CD8), treated or not with MV87 (10 mg/kg). Mean percentages ± SD of $n = 10$ animals. **B** and **C,** Tumor weight (gr; **B**) and number (**C**) of lung metastasis. **D,** Mean percentage ± SD of M-MDSCs (CD45$^+$CD11b$^+$Ly6G^{low}Ly6C^{high}) and PMN-MDSCs (CD45$^+$CD11b$^+$Ly6G^{high}Ly6C^{low}) in blood, spleen, and tumors of vehicle (CTRL) or MV87-treated WT or athymic tumor-bearing mice treated with anti-CD4/anti-CD8 antibodies. Mean percentages ± SD of $n = 10$ (*t* test: *, $P < 0.05$; **, $P < 0.01$; ***, $P < 0.001$). **E,** Impact of the NAMPT inhibitor MV87 on the anticancer activity of anti-PD-1 immunotherapy. Left, MN/MCA1 growth in mice treated with vehicle or MV87 (10 mg/kg) and/or anti-PD-1 (200 μg/mouse), tumor weight (gr; middle), and number of lung metastasis (right) were estimated. Mean percentages ± SD 4 mice/group (*t* test: *, $P < 0.05$; **, $P < 0.01$; ***$P < 0.001$). ns, nonsignificant.

Downloaded from cancerres.aacrjournals.org on February 4, 2020. © 2019 American Association for Cancer Research.

Published OnlineFirst February 18, 2019; DOI: 10.1158/0008-5472.CAN-18-1544

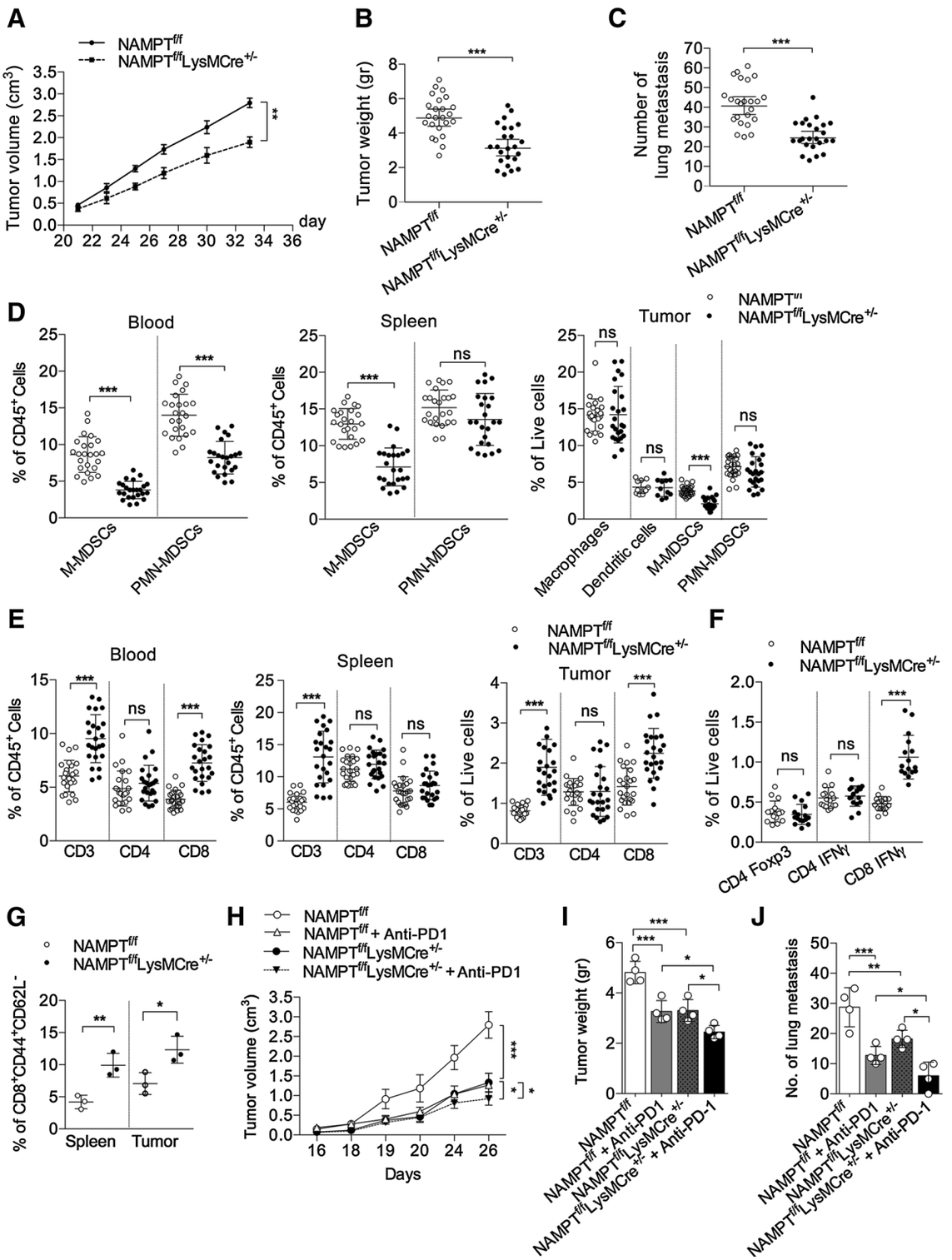

Figure 3.

Role of myeloid-specific NAMPT in tumor development. **A,** MN/MCA1 growth in NAMPT$^{f/f}$ and NAMPT$^{f/f}$LysMCre$^{\pm}$ mice. Mean percentages ± SD of three independent experiments (8 mice/group). **B** and **C,** Tumor weight (gr; **B**) and lung metastasis number (**C**) in NAMPT$^{f/f}$ and NAMPT$^{f/f}$LysMCre$^{\pm}$ tumor-bearing mice. Mean percentages ± SD of three independent experiments (8 mice/group). **D,** Mean percentage ± SD of M-MDSCs (CD45^{+}CD11b^{+}Ly6G^{low}Ly6C^{high}) and PMN-MDSCs (CD45^{+}CD11b^{+}Ly6G^{high}Ly6C^{low}) in blood, spleen, and tumors of NAMPT$^{f/f}$ and NAMPT$^{f/f}$LysMCre$^{\pm}$ tumor-bearing mice. (*Continued on the following page.*)

Downloaded from cancerres.aacrjournals.org on February 4, 2020. © 2019 American Association for Cancer Research.

Published OnlineFirst February 18, 2019; DOI: 10.1158/0008-5472.CAN-18-1544

the specific iNOS inhibitor L-NMMA (6). As a result, L-NMMA reduced both primary tumors and metastasis formation (Supplementary Fig. S4H).

In further support of the central role of NAMPT in the mobilization and functions of myeloid cells, accumulation of $CXCR4^+$ myeloid cells in the bone marrow was observed also in naïve $NAMPT^{f/f}LysMCre^{\pm}$ mice (Supplementary Fig. S4I) whereas, similarly with MDSCs, NAMPT-deficiency in tumor-associated macrophages resulted in increased levels of CXCR4 and reduced levels of iNOS (Supplementary Fig. S4J).

NAMPT inhibition restrains MDSC mobilization

To further clarify the mechanisms that promote the accumulation of MDSCs, we next investigated the effect of NAMPT inhibition on MDSC survival, differentiation, and mobilization from the bone marrow. Notably, purified bone marrow–resident monocytic and granulocytic cells, respectively, expressing the M-MDSCs ($CD45^+CD11b^+Ly6C^{high}Ly6G^{low}$) and PMN-MDSCs ($CD45^+CD11b^+Ly6C^{low}$ $Ly6G^{high}$) markers, treated *in vitro* with NAMPT inhibitors, were more resistant to FK866- or MV87-mediated cytotoxicity (Supplementary Fig. S5A) than cancer cells in the same condition (Supplementary Fig. S1A). Of note, the obtained IC_{50} values were likely above the dose reached *in vivo* ($IC_{50} = 95.6 \pm 12.7$ nmol/L for M-MDSCs; $IC_{50} = 212.3 \pm 46.2$ nmol/L for PMN-MDSCs). To evaluate the *in vitro* differentiation of MDSCs, bone marrow precursors were differentiated in the presence or absence of MV87 (10 nmol/L) or FK866 (10 nmol/L), in response to the differentiating factors IL6, GM-CSF, and G-CSF (28). No differences of the differentiated M-MDSCs and PMN-MDSCs populations were observed at any time point by flow cytometry as compared with controls (Supplementary Fig. S5B). Next, we investigated the hematopoietic response of $NAMPT^{f/f}LysMCre^{\pm}$ mice under both steady-state and emergency conditions (tumor growth), analyzing the commitment of hematopoietic progenitors (LK, CMP, GMP, and MEP) and their M-MDSCs and PMN-MDSCs progeny (Supplementary Fig. S5C–S5E). Under basal conditions, $NAMPT^{f/f}$ and $NAMPT^{f/f}LysMCre^{\pm}$ mice displayed comparable percentages of LK cells in the bone marrow, which similarly increased in tumor-bearing mice in both strains (Supplementary Fig. S5C). Nevertheless, the distribution of committed progenitors within the LK fraction was different between $NAMPT^{f/f}$ and $NAMPT^{f/f}LysMCre^{\pm}$ tumor-bearing mice, with a mild reduction in GMP (Supplementary Fig. S5D) and in bone marrow–derived PMN-MDSCs (Supplementary Fig. S5E) from $NAMPT^{f/f}LysMCre^{\pm}$ tumor-bearing mice. These results appear in agreement with the previously reported role of NAMPT in steady-state granulopoiesis (29). We then estimated the mobilization of MDSCs by measuring their frequency in the bone marrow of tumor-bearing mice and observed that following MV87 treatment, BM-$CD11b^+$ cells and both M- and PMN-MDSCs types were significantly increased, as compared with vehicle-treated animals (Fig. 4A), indicating that NAMPT inhibition blocks signals promoting the exit of MDSCs from the bone marrow. Supporting this evidence, a higher density of $CD11b^+$ myeloid elements and of M-MDSCs and PMN-MDSCs were observed in the bone marrow parenchyma of $NAMPT^{f/f}LysMCre^{\pm}$ tumor-bearing mice, as compared with their control $NAMPT^{f/f}$ counterpart (Fig. 4B).

Overall, these results suggested that the decreased frequency of MDSCs in the periphery and their accumulation in the bone marrow were ascribable to a defective mobilization from the bone marrow rather than to relevant modifications in the hematopoiesis. On the basis of these findings, we analyzed the expression of CXCR4, whose binding to CXCL12 provides a key axis for the retention of MDSCs into the bone marrow (30). Flow cytometry revealed that either pharmacologic inhibition (Fig. 4C, left) or genetic ablation (Fig. 4C, right) of *Nampt* results in a higher expression of CXCR4 in bone marrow–resident M-MDSCs and PMN-MDSCs, suggesting that NAMPT acts as a negative regulator of CXCR4 expression toward MDSCs in the bone marrow. Accordingly, while myeloid-specific ablation of NAMPT enhanced the number of M-MDSCs in the bone marrow and decreased their level in both peripheral blood and spleen, treatment with the CXCR4 antagonist AMD3100 overturned this phenotype by increasing the number of M-MDSCs in both peripheral blood and spleen of $NAMPT^{f/f}LysMCre^{\pm}$ mice and decreasing their retention in the bone marrow (Fig. 4D).

In accordance with the cytofluorimetric analysis (Fig. 3D), immunostaining of bone marrow, spleen, and tumor tissues confirmed that myeloid-specific ablation of NAMPT ($NAMPT^{f/f}$-$LysMCre^{\pm}$ mice) results in reduced accumulation of $IL4R^+$ suppressor myeloid cells (31) in the spleen, as opposed to increased CXCR4 expression in bone marrow–resident myeloid cells, further supporting the decreased CXCR4-dependent mobilization of myeloid cells from bone marrow to the periphery (Fig. 4E). Of relevance, the reduced mobilization of MDSCs to the periphery observed in $NAMPT^{f/f}LysMCre^{\pm}$ mice was paralleled by a significant increase in the number of tumor-infiltrating $CD3^+$ T cells (Fig. 4E). To validate the role of NAMPT in patients with cancer, we analyzed peripheral blood M-MDSCs from both healthy donors ($n = 8$) and patients with advanced colorectal cancer (stage II/III) ($n = 13$). As expected, the number of peripheral blood M-MDSCs ($CD14^+HLA\text{-}DR^{low/neg}CD33^+$) was increased in patients with colorectal cancer (Fig. 5A). The levels of M-MDSCs were not modulated by the *in vitro* treatment with MV87 (Fig. 5A), indicating the absence of toxicity. MDSCs from patients with colorectal cancer expressed significant levels of NAMPT (Fig. 5B) and MV87 treatment consistently reduced the expression of iNOS by these cells (Fig. 5C). Moreover, IFNγ induced a significant increase of NAMPT expression in monocytes from patients with colorectal cancer (Fig. 5D). Finally, treatment of both peripheral

(*Continued.*) The number of tumor macrophages ($CD45^+F4/80^+$) and dendritic cells ($CD45^+CD11b^+MHCII^+CD11c^+Ly6c^-$) is also shown. Mean percentages ± SD of three independent experiments (8 mice/group). **E,** Mean percentage ± SD of $CD3^+$ T cells ($CD45^+CD3^+$), $CD4^+$ T cells ($CD45^+CD4^+$), and $CD8^+$ T cells ($CD45^+CD8^+$) in blood, spleen, and tumors of $NAMPT^{f/f}$ and $NAMPT^{f/f}LysMCre^{\pm}$ tumor-bearing mice. Mean percentages ± SD of two independent experiments (8 mice/group). **F,** Flow cytofluorimetry analysis of Treg ($CD45^+CD4^+Foxp3^+$), $IFN\gamma^+CD4^+$ T cells ($CD45^+CD4^+IFN\gamma^+$), and $IFN\gamma^+CD8^+$ ($CD45^+CD8^+IFN\gamma^+$) T cells in tumors from $NAMPT^{f/f}$ and $NAMPT^{f/f}LysMCre^{\pm}$ tumor-bearing mice. Mean percentages ± SD of two independent experiments (8 mice/group). **G,** Flow cytofluorimetry analysis of $CD44^+CD62L^-$ effector/memory $CD8^+$ T-cell populations in spleen and tumor from $NAMPT^{f/f}$ and $NAMPT^{f/f}LysMCre^{\pm}$ mice. Mean percentages ± SD of one independent experiment (three mice/group). **H,** Impact of myeloid-specific ablation of *Nampt* on the anticancer activity of anti-PD-1 immunotherapy. MN/MCA1 growth $NAMPT^{f/f}$ and $NAMPT^{f/f}LysMCre^{\pm}$ mice treated or not with anti-PD-1 (200 μg/mouse). Tumor weight (gr; **I**) and number (**J**) of lung metastases were estimated. Mean percentages ± SD of 4 mice/group (*t* test: *, $P < 0.05$; **, $P < 0.01$; ***, $P < 0.001$). ns, nonsignificant.

Downloaded from cancerres.aacrjournals.org on February 4, 2020. © 2019 American Association for Cancer Research.

Published OnlineFirst February 18, 2019; DOI: 10.1158/0008-5472.CAN-18-1544

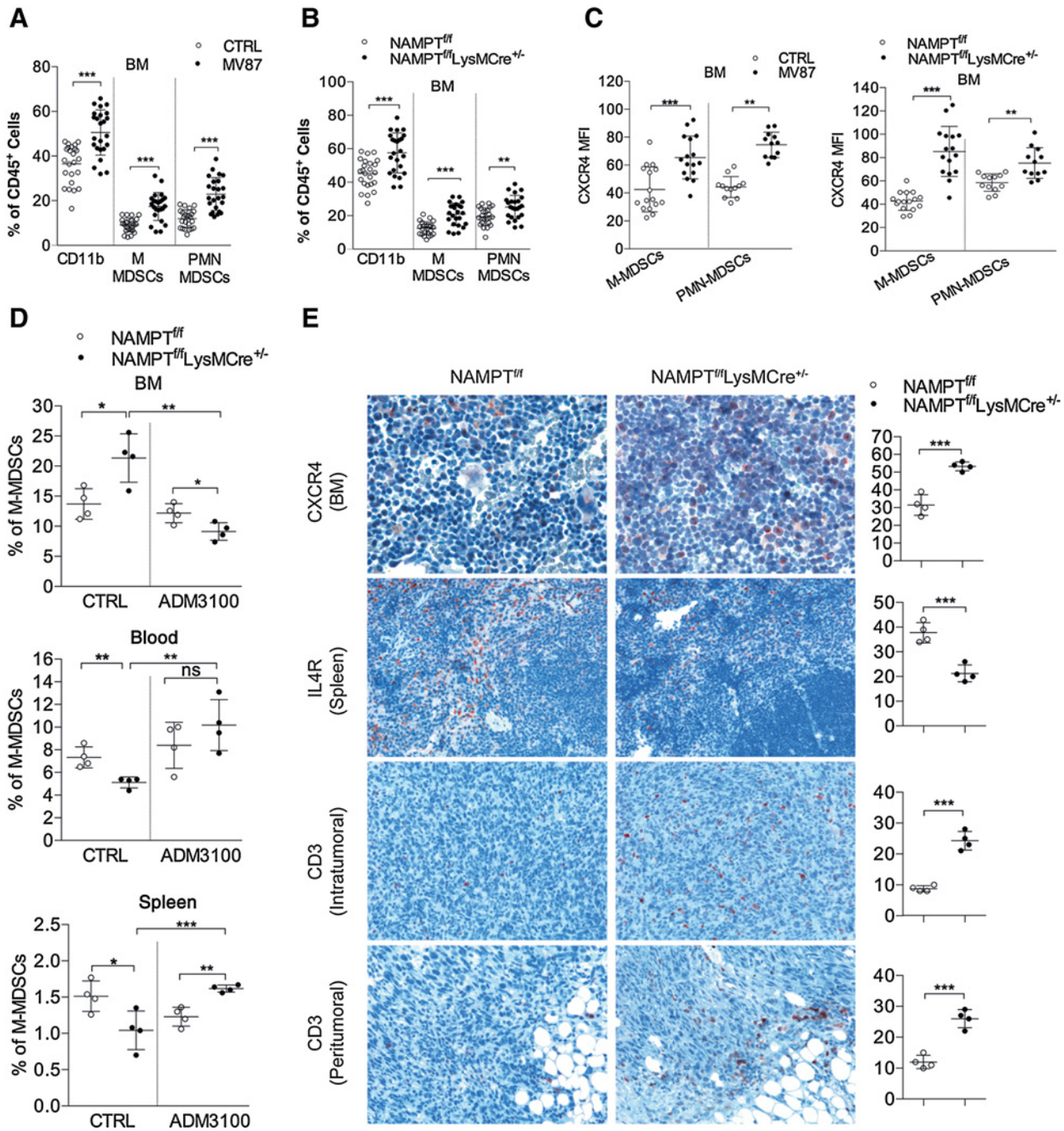

Figure 4.

NAMPT inhibitors reduce MDSCs mobilization. **A,** Mean percentage ± SD of CD11b$^+$ cells (CD45$^+$Cd11b$^+$), M-MDSCs (CD45$^+$CD11b$^+$Ly6G^{low}Ly6C^{high}), and PMN-MDSCs (CD45$^+$CD11b$^+$Ly6G^{high}Ly6C^{low}) in the bone marrow of vehicle or MV87-treated tumor-bearing mice. Mean percentages ± SD of three independent experiments (8 mice/group). **B,** Percentage of CD11b$^+$ cells (CD45$^+$Cd11b$^+$), M-MDSCs (CD45$^+$CD11b$^+$Ly6G^{low}Ly6C^{high}), and PMN-MDSCs (CD45$^+$CD11b$^+$Ly6G^{high}Ly6C^{low}) in in the bone marrow of NAMPT$^{f/f}$ and NAMPT$^{f/f}$LysMCre$^{\pm}$ tumor-bearing mice. Mean percentages ± SD of three independent experiments (8 mice/group). **C,** Mean ± SD of CXCR4 expression in M-MDSCs (CD45$^+$CD11b$^+$Ly6G^{low}Ly6C^{high}) and PMN-MDSCs (CD45$^+$CD11b$^+$Ly6G^{high}Ly6C^{low}) in the bone marrow of vehicle or MV87-treated tumor-bearing WT mice (left) and in the bone marrow of NAMPT$^{f/f}$ and NAMPT$^{f/f}$LysMCre$^{\pm}$ tumor-bearing mice (right). Mean percentages ± SD of two independent experiments (8 mice/group). **D,** Percentage of M-MDSCs in bone marrow, blood, spleen of NAMPT$^{f/f}$ and NAMPT$^{f/f}$LysMCre$^{\pm}$ tumor-bearing mice, treated or not with the CXCR4 antagonist ADM3100. Flow cytofluorimetry analysis estimated within the CD45$^+$ gate. Mean percentages ± SD of four mice/group. **E,** Histopathologic analysis of CXCR4, IL4R, and CD3 in bone marrow, spleen, and tumor tissues from NAMPT$^{f/f}$ and NAMPT$^{f/f}$LysMCre$^{\pm}$ tumor-bearing mice (left). Right, relative quantitative analysis, $n = 4$ (t test: *, $P < 0.05$; **, $P < 0.01$; ***, $P < 0.001$). ns, nonsignificant.

Downloaded from cancerres.aacrjournals.org on February 4, 2020. © 2019 American Association for Cancer Research.

Published OnlineFirst February 18, 2019; DOI: 10.1158/0008-5472.CAN-18-1544

blood monocytes and M-MDSCs from patients with colorectal cancer resulted in increased surface expression of CXCR4 (Fig. 5E). Along with the observations obtained in mice, these results suggest a role of NAMPT in the regulation of the mobilization of suppressive human M-MDSCs.

NAMPT is part of an M-CSF/NAMPT/SIRT1/HIF1α/CXCR4 axis controlling MDSC mobilization

Because CXCR4 expression is under the control of HIF1α activity (32) and SIRT1 acts as an inhibitor of HIF1α transcriptional activity (18), we next investigated whether NAMPT could

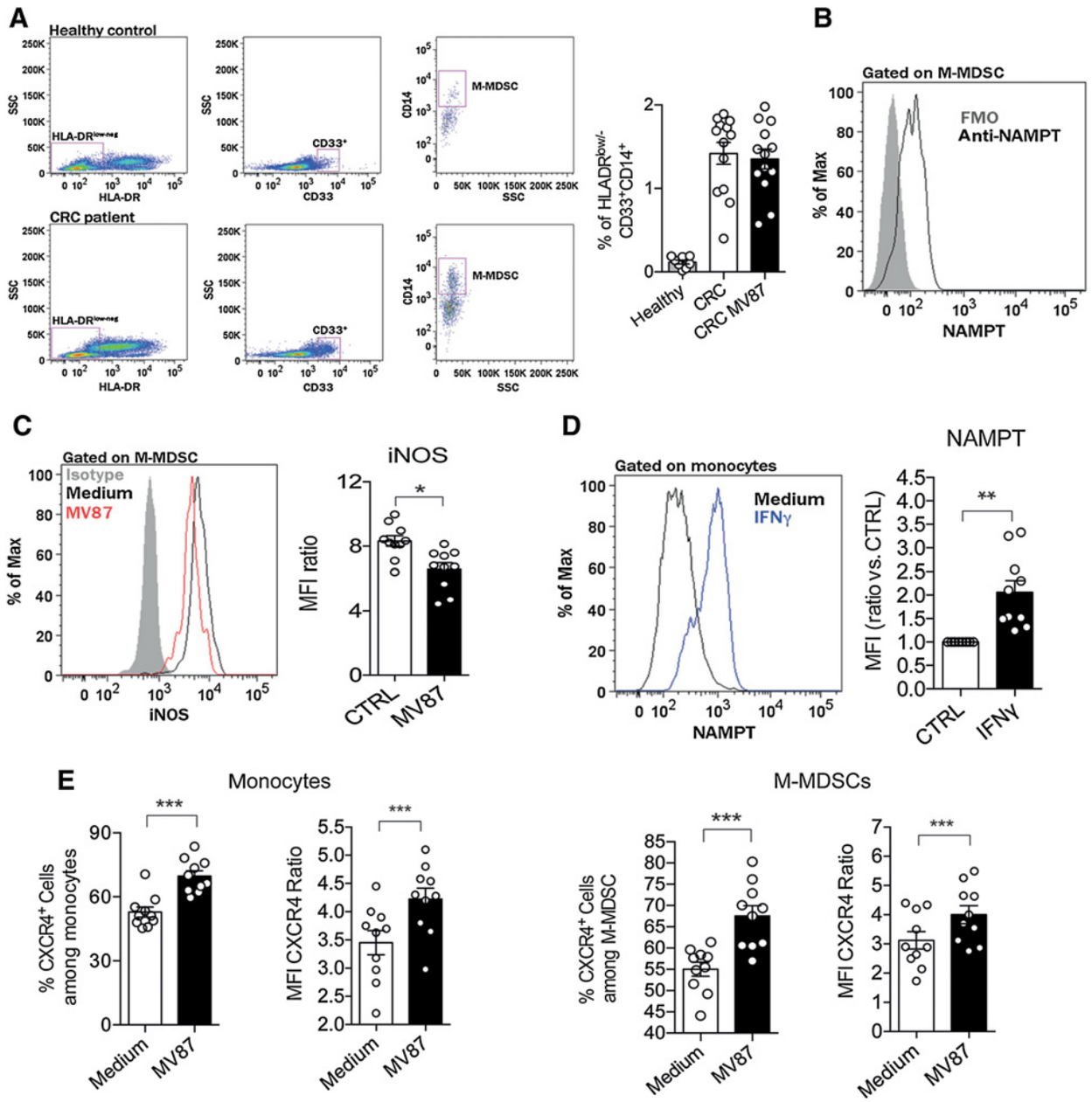

Figure 5.

Functional expression of NAMPT in human M-MDSCs from patients with colorectal cancer. **A,** Left, gating strategy used to determine M-MDSCs in human PBMC. Right, mean percentages ± SD of M-MDSCs ($CD14^+HLA\text{-}DR^{low/neg}CD33^+$) in blood from healthy donors ($n = 8$) and patients with colorectal cancer ($n = 13$) treated or not with MV87 (10 nmol/L) for 16 hours. **B,** Representative flow cytometry analysis of NAMPT expression in human M-MDSCs from patients with colorectal cancer. **C,** Flow cytometry analysis (left) and mean ± SD of iNOS expression (right) in human M-MDSCs ($CD14^+HLA\text{-}DR^{low/neg}CD33^+$) from patients with colorectal cancer, treated or not with MV87 (10 nmol/L) for 16 hours ($n = 10$). **D,** Representative flow cytometry analysis (left) and mean fluorescence intensity (MFI) ± SD of NAMPT expression (right) in $CD14^+$ monocytes stimulated or not with IFNγ for 16 hours ($n = 10$ patients). **E,** Flow cytofluorimetry analysis of CXCR4 expression (MFI) in peripheral blood monocytes and M-MDSCs from patients with colorectal cancer. Cells were treated with either vehicle (CTRL) or the NAMPT inhibitor MV87 (10 nmol/L) for 48 hours, as indicated. Mean percentages ± SD of 10 independent experimental points (patients; *t* test: *, $P < 0.05$; ***, $P < 0.001$).

Downloaded from cancerres.aacrjournals.org on February 4, 2020. © 2019 American Association for Cancer Research.

Published OnlineFirst February 18, 2019; DOI: 10.1158/0008-5472.CAN-18-1544

hamper the HIF1α–induced CXCR4 gene expression. In agreement with this hypothesis, while myeloid-specific ablation of HIF1α (HIF1α$^{f/f}$LysMCre$^{+/-}$) reduced the surface expression of CXCR4 in bone marrow–resident M- and PMN-MDSCs (Fig. 6A), ablation of SIRT1 in bone marrow cells isolated from SIRT1$^{f/f}$-LysMCre$^{+/-}$ mice resulted in increased levels of CXCR4 surface expression (Fig. 6B). Also, mRNA levels of the prototypical hypoxia-inducible genes *CXCR4* and VEGF were decreased in BM M-MDSCs from HIF1α$^{f/f}$LysMCre$^{+/-}$ mice (Fig. 6C) and, conversely, increased in bone marrow M-MDSCs from either SIRT1$^{f/f}$LysMCre$^{+/-}$ or NAMPT$^{f/f}$LysMCre$^{\pm}$ mice (Fig. 6C). Further in agreement, NAMPT ablation reduced *Sirt1* mRNA levels,

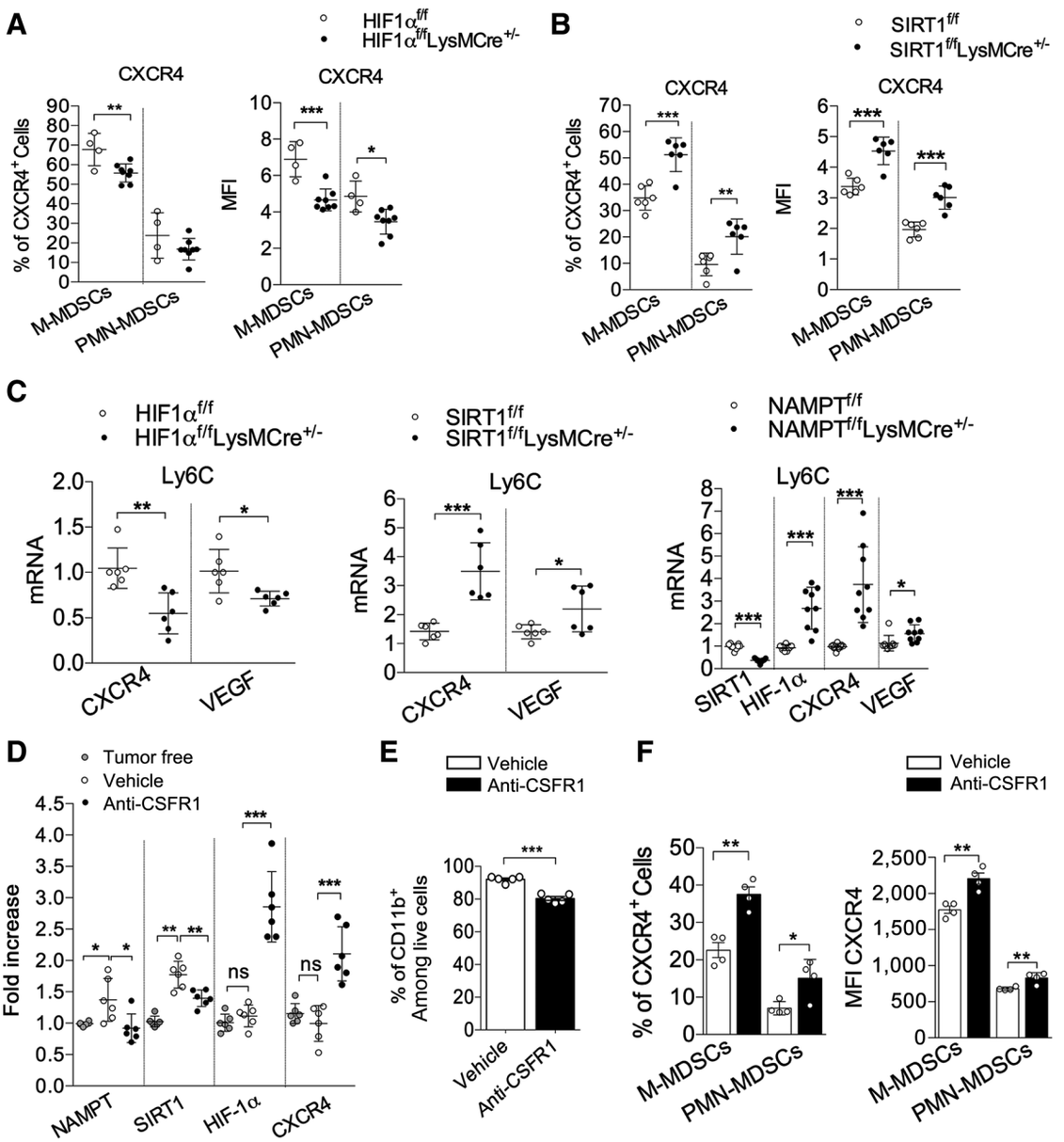

Figure 6.

M-CSF guides NAMPT-mediated CXCR4 inhibition. **A,** Mean ± SD of CXCR4 expression in BM M-MDSCs (CD45$^+$CD11b$^+$Ly6G^{low}Ly6C^{high}) and PMN-MDSCs (CD45$^+$CD11b$^+$Ly6G^{high}Ly6C^{low}) from HIF1α$^{f/f}$ ($n = 4$) and HIF1α$^{f/f}$LysMCre$^{\pm}$ ($n = 8$). **B,** Representative cytometry analysis of CXCR4 expression in BM M-MDSCs (CD45$^+$CD11b$^+$Ly6G^{low}Ly6C^{high}) and PMN-MDSCs (CD45$^+$CD11b$^+$Ly6G^{high}Ly6C^{low}) from SIRT1$^{f/f}$ ($n = 6$) and SIRT1$^{f/f}$LysMCre$^{\pm}$ mice ($n = 6$). **C,** Left, mRNA expression levels of *Cxcr4, Vegf,* in BM-M-MDSCs from HIF1α$^{f/f}$ and HIF1α$^{f/f}$LysMCre$^{\pm}$ mice, $n = 6$; middle, mRNA expression levels of *Cxcr4, Vegf* in BM-M-MDSCs from SIRT1$^{f/f}$ and SIRT1$^{f/f}$LysMCre$^{\pm}$ mice, $n = 6$; right, mRNA expression levels of *Sirt1, HIF1α, Vegf, and Cxcr4,* in BM-M-MDSCs from NAMPT$^{f/f}$ and NAMPT$^{f/f}$LysMCre$^{\pm}$ mice, $n = 9$. **D,** mRNA levels of *Nampt, Sirt1, HIF1α*, and *Cxcr4* in bone marrow CD11b$^+$ cells from tumor-bearing mice treated or not with anti-CSFR1 antibody, $n = 6$. **E,** CD11b$^+$ cells in blood of untreated (vehicle) and treated (anti-CSFR1 antibody) tumor-bearing mice, $n = 5$. **F,** Percentage and mean fluorescence intensity (MFI) of CXCR4$^+$ monocytic (CD45$^+$ CD11b$^+$Ly6C^{high}Ly6G^{low}) and granulocytic (CD45$^+$CD11b$^+$Ly6G^{high}Ly6C^{low}) MDSCs in bone marrow from untreated (vehicle) and treated (anti-CSF1R antibody) tumor-bearing mice, $n = 4$ (*t* test: *, $P < 0.05$; **, $P < 0.01$; ***, $P < 0.001$). ns, nonsignificant.

Downloaded from cancerres.aacrjournals.org on February 4, 2020. © 2019 American Association for Cancer Research.

Published OnlineFirst February 18, 2019; DOI: 10.1158/0008-5472.CAN-18-1544

increasing *HIF1α*, *Cxcr4*, and *Vegf* mRNAs (Fig. 6C). Expression analysis of additional genes (Supplementary Fig. S6A) involved in angiogenesis (i.e., *CXCL12*) and cancer-related inflammation (i.e., *IL6*) showed that HIF1α deficiency (HIF1α$^{f/f}$LysCre$^{+/-}$) decreases their expression, while in agreement either SIRT1 (SIRT1$^{f/f}$LysCre$^{+/-}$) or NAMPT deficiency (NAMPT$^{f/f}$LysCre$^{+/-}$) produced a specular phenotype, with increased expression of both *CXCL12* and *IL6*. Furthermore, in support of the antagonist role between HIF1α and the NAMPT/Sirt1 axis, whereas HIF1α deficiency produced an increase in TGFβ and IL10, the lack of SIRT1 or NAMPT decreased both genes.

Given the central role of M-CSF in supporting both expansion and the tumor-promoting activity of myeloid cells (2, 33), we next investigated its relevance in NAMPT-mediated mobilization of myeloid cells. To this aim, tumor-bearing mice were treated or not with an anti-CSFR1 antibody (33). Untreated BM-CD11b$^+$ myeloid cells displayed increased *Nampt* mRNA expression in comparison with the tumor-free counterpart, whereas the anti-CSFR1 treatment reduced the mRNA levels of both *Nampt* and *Sirt1* genes, while in contrast increased the levels of HIF1α and C*xcr4* mRNA (Fig. 6D). Accordingly, the anti-CSFR1 antibody decreased the number of CD11b$^+$ cells in peripheral blood (Fig. 6E), while increased the level of CXCR4$^+$ M- and PMN-MDSCs in the bone marrow (Fig. 6F). To further strengthen the causal association between M-CSF and NAMPT activity, we assessed whether the effects elicited by the anti-CSFR1 treatment *in vivo* were lost in NAMPT-ablated mice. As shown in Supplementary Fig. S6B, the accumulation of MDSCs in the bone marrow, as well as their reduction in the periphery, observed in NAMPT$^{f/f}$ mice in response to the anti-CSFR treatment, was lost in NAMPT$^{f/f}$-LysCre$^{+/-}$ mice, where only a poor reduction of splenic M-MDSCs was still observable. In support of a role of myeloid growth factors as regulators of NAMPT-mediated myeloid cell mobilization, a similar phenotype was obtained in G-CSFR–deficient mice (Supplementary Fig. S6C). Hence, in cancer bearers, a sequence of events guided by myeloid growth factors (i.e., M-CSF) support the increased hematopoietic output by enhancing both differentiation and mobilization of myeloid cells, the latter through a NAMPT/SIRT1–dependent inactivation of HIF-α–mediated *CXCR4* gene transcription, eventually culminate with the peripheral accumulation of myeloid suppressor cells.

Discussion

These results provide evidence that in cancer, a multistep metabolic process is guided by increased levels of NAMPT, in response to myeloid growth factors (i.e., M-CSF, G-CSF; refs. 2, 6). This process results in the inactivation of the CXCR4-dependent retention axis and mobilization of suppressor myeloid populations toward tumor immune suppression. In support, pharmacologic inhibition or genetic ablation of NAMPT in the myeloid compartment invariably reduced tumor growth and metastasis formation, while enhancing the antitumor efficacy of immune checkpoint inhibitors (i.e. anti-PD-1). The control operated by NAMPT over the mobilization of hematopoietic precursors appears particularly relevant in emergency hematopoiesis (e.g., infection and cancer), when extensive myeloid progenitors proliferate in response to myeloid growth factors increasing the local oxygen consumption and stabilizing the hypoxia-inducible factor HIF1α (34) and, in turn, promoting the CXCR4/CXCL12–mediated retention of myeloid cells (31–35). However, accumulation of CXCR4$^+$ myeloid cells in the bone marrow was also observed in naïve NAMPT$^{f/f}$LysMCre$^{\pm}$ mice, further highlighting the key role of NAMPT in the control of myeloid cells' mobilization. The NAMPT-induced NAD-dependent SIRT1 activity represents a crucial repressor mechanism of HIF1α target genes (18), CXCR4 included. Alternatively, whereas CXCR4 is strongly induced by ROS (36), NAMPT inhibition results in reduced ROS production (37), which coincides with the reduction of CXCR4. Our observation integrates a previous report showing that the NAMPT–NAD$^+$–SIRT1 pathway promotes activation of C/EBP-α and C/EBP-β–driven G-CSF and G-CSFR genes' transcription, and indicates that in addition to granulopoiesis (29), NAMPT orchestrates the redistribution of myeloid cells. Furthermore, whereas NAMPT inhibitors provide a therapeutic opportunity to limit cancer immunosuppression, NAMPT agonists (38) might integrate standard mobilization regimens (e.g., G-CSF) to deliver hematopoietic support in conditions of leukopenia (39). Of relevance, in agreement with Audrito and colleagues (40), we observed that NAMPT is induced by M1-polarizing signals. In this regard, an antagonistic cross-talk was reported between M1-related inflammatory programs and SIRT1 (41), which may support a homeostatic regulation operated by the NAMPT–NAD$^+$–SIRT1 pathway through the activation of M2 inflammation (40). Furthermore, because we have observed that NAMPT-deficient tumor-associated macrophages express increased levels of CXCR4 and reduced levels of iNOS, the role of NAMPT may likely go beyond the regulation of MDSC mobilization and is likely to affect the tumor microenvironment. Of interest, the cytotoxic action elicited by NAMPT inhibitors on tumor cells, along with their capacity to reactivate the specific antitumor immunity, could promote a further effort for the development of new antagonists of NAMPT, which, if deprived of toxicity, could act as double-edged swords against neoplasms.

Overall, the identification of NAMPT as an upstream metabolic hub controlling mobilization and functions of MDSCs provides new opportunities to reverse tumor immunosuppression and retrieve the clinical efficacy of immunotherapy in nonresponder patients with cancer.

Disclosure of Potential Conflicts of Interest

C. Travelli reports receiving other commercial research support. No potential conflicts of interest were disclosed by the other authors.

Authors' Contributions

Conception and design: C. Travelli, A.A. Genazzani, A. Sica
Development of methodology: C. Travelli, S. Morlacchi, A.A. Grolla, A. Sica
Acquisition of data (provided animals, acquired and managed patients, provided facilities, etc.): C. Travelli, F.M. Consonni, S. Sangaletti, M. Storto, P. Portararo, L. Rimassa, T. Pressiani, M. Mazzone, R. Trovato, S. Ugel, C. Tripodo, A. Sica
Analysis and interpretation of data (e.g., statistical analysis, biostatistics, computational analysis): C. Travelli, C. Tripodo, A.A. Genazzani, A. Sica
Writing, review, and/or revision of the manuscript: C. Travelli, L. Rimassa, T. Pressiani, M. Mazzone, V. Bronte, C. Tripodo, M.P. Colombo, A.A. Genazzani, A. Sica
Administrative, technical, or material support (i.e., reporting or organizing data, constructing databases): C. Travelli
Study supervision: A.A. Genazzani, A. Sica
Other (design and synthesis of the compounds used in this project): U. Galli, G.C. Tron

Downloaded from cancerres.aacrjournals.org on February 4, 2020. © 2019 American Association for Cancer Research.

Published OnlineFirst February 18, 2019; DOI: 10.1158/0008-5472.CAN-18-1544

Acknowledgments

We thank Professor Oberdan Leo for providing us the NAMPT$^{f/f}$ strain. We thank Dr. Carmen Correale for manuscript editing and Dr. Andrea Ponzetta for technical suggestions. We thank Dr. Giuseppe Orsomando for providing us the G217R_NAMPT construct. We thank Dr. Simone Torretta for help in the generation of MN-MCA1 G217R cell line and Dr. Rita de Sanctis for providing us human blood samples. This work was supported by: Associazione Italiana Ricerca sul Cancro (AIRC) Program Innovative Tools for Cancer Risk Assessment and Diagnosis, 5 per mille number 12162 (to C. Tripodo and M.P. Colombo) and IG number 14194 (to M.P. Colombo), 15585 (to A. Sica) and 19885 (to A. Sica); AIRC, fellowship "Pierluigi Meneghelli", project code 19682 (to F. Consonni); Leonino Fontana e Maria Lionello Fellowship, project code 14832 (to C. Travelli); SIF-Takeda grant in Pharmaceutical oncology (to C. Travelli); Fondazione Veronesi Fellowship 2018 (to C. Travelli); grant from the Fondazione San Paolo, Dipartimento di Scienze del Farmaco, Università del Piemonte Orientale, Novara, 28100; Fondazione Cariplo (to A. Sica), and Ministero Università Ricerca (MIUR; to A. Sica).

The costs of publication of this article were defrayed in part by the payment of page charges. This article must therefore be hereby marked *advertisement* in accordance with 18 U.S.C. Section 1734 solely to indicate this fact.

Received May 19, 2018; revised December 31, 2018; accepted February 13, 2019; published first February 18, 2019.

References

1. Sica A, Bronte V. Altered macrophage differentiation and immune dysfunction in tumor development. J Clin Invest 2007;117:1155–66.
2. Strauss L, Sangaletti S, Consonni FM, Szebeni G, Morlacchi S, Totaro MG, et al. RORC1 regulates tumor-promoting "Emergency" Granulo-Monocytopoiesis. Cancer Cell 2015;28:253–69.
3. Movahedi K, Guilliams M, Van den Bossche J, Van den Bergh R, Gysemans C, Beschin A, et al. Identification of discrete tumor-induced myeloid-derived suppressor cell subpopulations with distinct T cell-suppressive activity. Blood 2008;111:4233–44.
4. Nagaraj S, Collazo M, Corzo CA, Youn JI, Ortiz M, Quiceno D, et al. Regulatory myeloid suppressor cells in health and disease. Cancer Res 2009;69:7503–6.
5. Sica A, Mantovani A. Macrophage plasticity and polarization: in vivo veritas. J Clin Invest 2012;122:787–95.
6. Gabrilovich DI, Ostrand-Rosenberg S, Bronte V. Coordinated regulation of myeloid cells by tumours. Nat Rev Immunol 2012;12:253–68.
7. Shojaei F, Wu X, Zhong C, Yu L, Liang XH, Yao J, et al. Bv8 regulates myeloid-cell-dependent tumour angiogenesis. Nature 2007;450:825–31.
8. Cui TX, Kryczek I, Zhao L, Zhao E, Kuick R, Roh MH, et al. Myeloid-derived suppressor cells enhance stemness of cancer cells by inducing microRNA101 and suppressing the corepressor CtBP2. Immunity 2013;39:611–21.
9. Diaz-Montero CM, Salem ML, Nishimura MI, Garrett-Mayer E, Cole DJ, Montero AJ. Increased circulating myeloid-derived suppressor cells correlate with clinical cancer stage, metastatic tumor burden, and doxorubicin-cyclophosphamide chemotherapy. Cancer Immunol Immunother 2009;58:49–59.
10. Foudi A, Jarrier P, Zhang Y, Wittner M, Geay JF, Lecluse Y, et al. Reduced retention of radioprotective hematopoietic cells within the bone marrow microenvironment in CXCR4-/- chimeric mice. Blood 2006;107:2243–51.
11. Peled A, Abraham M, Avivi I, Rowe JM, Beider K, Wald H, et al. The high-affinity CXCR4 antagonist BKT140 is safe and induces a robust mobilization of human CD34+ cells in patients with multiple myeloma. Clin Cancer Res 2014;20:469–79.
12. Pan PY, Wang GX, Yin B, Ozao J, Ku T, Divino CM, et al. Reversion of immune tolerance in advanced malignancy: modulation of myeloid-derived suppressor cell development by blockade of stem-cell factor function. Blood 2008;111:219–28.
13. Suzuki E, Kapoor V, Jassar AS, Kaiser LR, Albelda SM. Gemcitabine selectively eliminates splenic Gr-1+/CD11b+ myeloid suppressor cells in tumor-bearing animals and enhances antitumor immune activity. Clin Cancer Res 2005;11:6713–21.
14. Serafini P, Meckel K, Kelso M, Noonan K, Califano J, Koch W, et al. Phosphodiesterase-5 inhibition augments endogenous antitumor immunity by reducing myeloid-derived suppressor cell function. J Exp Med 2006;203:2691–702.
15. Hammami I, Bertrand M, Chen J, Bronte V, De Crescenzo G, Jolicoeur M. Nitric oxide affects immune cells bioenergetics: long-term effects of nitric-oxide derivatives on leukaemic Jurkat cell metabolism. Immunobiology 2012;217:808–15.
16. Burgos ES, Vetticatt MJ, Schramm VL. Recycling nicotinamide. The transition-state structure of human nicotinamide phosphoribosyltransferase. J Am Chem Soc 2013;135:3485–93.
17. Chiarugi A, Dolle C, Felici R, Ziegler M. The NAD metabolome–a key determinant of cancer cell biology. Nat Rev Cancer 2012;12:741–52.
18. Lim JH, Lee YM, Chun YS, Chen J, Kim JE, Park JW. Sirtuin 1 modulates cellular responses to hypoxia by deacetylating hypoxia-inducible factor 1alpha. Mol Cell 2010;38:864–78.
19. Liu G, Bi Y, Shen B, Yang H, Zhang Y, Wang X, et al. SIRT1 limits the function and fate of myeloid-derived suppressor cells in tumors by orchestrating HIF1α-dependent glycolysis. Cancer Res 2014;74:727–37.
20. Galli U, Travelli C, Massarotti A, Fakhfouri G, Rahimian R, Tron GC, et al. Medicinal chemistry of nicotinamide phosphoribosyltransferase (NAMPT) inhibitors. J Med Chem 2013;56:6279–96.
21. Garten A, Petzold S, Korner A, Imai S, Kiess W. Nampt: linking NAD biology, metabolism and cancer. Trends Endocrinol Metab 2009;20:130–8.
22. Mantovani A, Allavena P, Sica A, Balkwill F. Cancer-related inflammation. Nature 2008;454:436–44.
23. Travelli C, Aprile S, Rahimian R, Grolla AA, Rogati F, Bertolotti M, et al. Identification of novel triazole-based nicotinamide phosphoribosyltransferase (NAMPT) inhibitors endowed with antiproliferative and antiinflammatory activity. J Med Chem 2017;60:1768–92.
24. Aslakson CJ, Miller FR. Selective events in the metastatic process defined by analysis of the sequential dissemination of subpopulations of a mouse mammary tumor. Cancer Res 1992;52:1399–405.
25. Watson M, Roulston A, Belec L, Billot X, Marcellus R, Bedard D, et al. The small molecule GMX1778 is a potent inhibitor of NAD+ biosynthesis: strategy for enhanced therapy in nicotinic acid phosphoribosyltransferase 1-deficient tumors. Mol Cell Biol 2009;29:5872–88.
26. Ribas A. Tumor immunotherapy directed at PD-1. N Engl J Med 2012;366:2517–9.
27. Blagih J, Jones RG. Polarizing macrophages through reprogramming of glucose metabolism. Cell Metab 2012;15:793–5.
28. Marigo I, Bosio E, Solito S, Mesa C, Fernandez A, Dolcetti L, et al. Tumor-induced tolerance and immune suppression depend on the C/EBPbeta transcription factor. Immunity 2010;32:790–802.
29. Skokowa J, Lan D, Thakur BK, Wang F, Gupta K, Cario G, et al. NAMPT is essential for the G-CSF-induced myeloid differentiation via a NAD(+)-sirtuin-1-dependent pathway. Nat Med 2009;15:151–8.
30. Ma Q, Jones D, Springer TA. The chemokine receptor CXCR4 is required for the retention of B lineage and granulocytic precursors within the bone marrow microenvironment. Immunity 1999;10:463–71.
31. Gallina G, Dolcetti L, Serafini P, De Santo C, Marigo I, Colombo MP, et al. Tumors induce a subset of inflammatory monocytes with immunosuppressive activity on CD8+ T cells. J Clin Invest 2006;116:2777–90.
32. Schioppa T, Uranchimeg B, Saccani A, Biswas SK, Doni A, Rapisarda A, et al. Regulation of the chemokine receptor CXCR4 by hypoxia. J Exp Med 2003;198:1391–402.
33. Ries CH, Cannarile MA, Hoves S, Benz J, Wartha K, Runza V, et al. Targeting tumor-associated macrophages with anti-CSF-1R antibody reveals a strategy for cancer therapy. Cancer Cell 2014;25:846–59.

Downloaded from cancerres.aacrjournals.org on February 4, 2020. © 2019 American Association for Cancer Research.

Published OnlineFirst February 18, 2019; DOI: 10.1158/0008-5472.CAN-18-1544

34. Levesque JP, Winkler IG, Hendy J, Williams B, Helwani F, Barbier V, et al. Hematopoietic progenitor cell mobilization results in hypoxia with increased hypoxia-inducible transcription factor-1 alpha and vascular endothelial growth factor A in bone marrow. Stem Cells 2007;25:1954–65.
35. Morikawa T, Takubo K. Hypoxia regulates the hematopoietic stem cell niche. Pflugers Arch 2015 Oct 21 [Epub ahead of print].
36. Saccani A, Saccani S, Orlando S, Sironi M, Bernasconi S, Ghezzi P, et al. Redox regulation of chemokine receptor expression. Proc Natl Acad Sci U S A 2000;97:2761–6.
37. Montecucco F, Bauer I, Braunersreuther V, Bruzzone S, Akhmedov A, Luscher TF, et al. Inhibition of nicotinamide phosphoribosyltransferase reduces neutrophil-mediated injury in myocardial infarction. Antioxid Redox Signal 2013;18:630–41.
38. Wang G, Han T, Nijhawan D, Theodoropoulos P, Naidoo J, Yadavalli S, et al. P7C3 neuroprotective chemicals function by activating the rate-limiting enzyme in NAD salvage. Cell 2014;158:1324–34.
39. Bendall LJ, Bradstock KF. G-CSF: from granulopoietic stimulant to bone marrow stem cell mobilizing agent. Cytokine Growth Factor Rev 2014;25:355–67.
40. Audrito V, Serra S, Brusa D, Mazzola F, Arruga F, Vaisitti T, et al. Extracellular nicotinamide phosphoribosyltransferase (NAMPT) promotes M2 macrophage polarization in chronic lymphocytic leukemia. Blood 2015;125:111–23.
41. Kauppinen A, Suuronen T, Ojala J, Kaarniranta K, Salminen A. Antagonistic crosstalk between NF-kappaB and SIRT1 in the regulation of inflammation and metabolic disorders. Cell Signal 2013;25:1939–48.

Downloaded from cancerres.aacrjournals.org on February 4, 2020. © 2019 American Association for Cancer Research.

Published OnlineFirst February 18, 2019; DOI: 10.1158/0008-5472.CAN-18-1544

Cancer Research
The Journal of Cancer Research (1916–1930) | The American Journal of Cancer (1931–1940)

AACR American Association for Cancer Research

Nicotinamide Phosphoribosyltransferase Acts as a Metabolic Gate for Mobilization of Myeloid-Derived Suppressor Cells

Cristina Travelli, Francesca Maria Consonni, Sabina Sangaletti, et al.

Cancer Res 2019;79:1938-1951. Published OnlineFirst February 18, 2019.

Updated version	Access the most recent version of this article at: doi:10.1158/0008-5472.CAN-18-1544
Supplementary Material	Access the most recent supplemental material at: http://cancerres.aacrjournals.org/content/suppl/2019/02/16/0008-5472.CAN-18-1544.DC1

Cited articles	This article cites 40 articles, 13 of which you can access for free at: http://cancerres.aacrjournals.org/content/79/8/1938.full#ref-list-1

E-mail alerts	Sign up to receive free email-alerts related to this article or journal.
Reprints and Subscriptions	To order reprints of this article or to subscribe to the journal, contact the AACR Publications Department at pubs@aacr.org.
Permissions	To request permission to re-use all or part of this article, use this link http://cancerres.aacrjournals.org/content/79/8/1938. Click on "Request Permissions" which will take you to the Copyright Clearance Center's (CCC) Rightslink site.

Downloaded from cancerres.aacrjournals.org on February 4, 2020. © 2019 American Association for Cancer Research.